CONF-9609283--2
ANL/PHY/CP--89699

Nondipolar photoelectron angular distributions

B. Krässig, M. Jung, D. S. Gemmell, E. P. Kanter, T. LeBrun, S. H. Southworth, and L. Young

Physics Division, Argonne National Laboratory, Argonne, IL 60439, USA

Abstract. The deviations of photoelectron angular distributions from the simple, highly symmetric shapes predicted within the electric-dipole approximation are investigated. The admixture of an electric-quadrupole component in the photon-atom interaction causes an asymmetry in the angular distribution with respect to the direction of photon propagation. The reported measurement of the angular distributions of argon 1*s*, krypton 2*s*, and krypton 2*p* photoemission within 2–3 keV above their respective thresholds reveal pronounced asymmetries which are present even at low electron kinetic energies. The measured asymmetry parameters are in good agreement with recent predictions from nonrelativistic calculations.

INTRODUCTION

The interaction of low-energy to soft x-ray photons with matter has largely been studied within the framework of the dipole approximation. This approximation is used when the photon's wavelength can be regarded large in comparison to the atomic dimensions. Consequently, the photon momentum, being proportional to inverse of the wavelength, is considered small and the dependence on the photon momentum is neglected. The photoelectron angular distribution in dipole approximation therefore remains unchanged if the direction of photon propagation is reversed. An extensive body of both theoretical and experimental work is concerned with the physical information that can be extracted from angular distributions in cases where the dipole approximation is valid (cf. the reviews [1, 2]).

With increasing energy the forward-backward symmetry in the angular distributions disappears. The first measurements of photoelectron angular distributions in the 1920s, using high-energy x rays, displayed pronounced forward

DISCLAIMER

peaking of the distributions [3, 4]. It was shown that this could be related to the momentum of the absorbed radiation, however not in such a way, as one might assume, that the emitted electrons are simply kicked forward by the photon momentum [5]. The dependence on the photon momentum is retained when the photon wave's exponential is approximated by the first two terms, $e^{i\mathbf{k}\cdot\mathbf{r}} \sim 1 + i\mathbf{k}\cdot\mathbf{r}$, rather than only by the unit term. This expansion of the exponential has a close correspondence to the multipole decomposition of the photon-atom interaction: the unit term leads to the long-wavelength limit of electric-dipole (E1) interaction, and the term linear in kr is related to magnetic-dipole (M1) and electric-quadrupole (E2) interactions. It is those additional contributions which are responsible for the observed forward-backward asymmetry in the angular distributions. In the early calculations, based on a hydrogenic model, this "retardation" effect was found to be proportional to v/c, in agreement with the experimental observations (cf. [6]).

Since the early papers relatively few theoretical and even fewer experimental studies have been reported on this subject. On the theoretical side, both relativistic and nonrelativistic calculations were performed for a variety of cases using a more refined model [7, 8]. On the experimental side, however, progress in this field had been hampered by the restriction to the limited spectrum and intensity obtained from the x-ray sources used (cf. [9]; for a listing of experiments before 1978, see [10]). With the availability of intense and tunable x-ray radiation at high-energy synchrotron radiation facilities, renewed interest for the topic has emerged. Recently, theoretical predictions of nondipolar angular distributions have been reported which differ significantly from the simpler retardation result, particularly for low photoelectron energies [11, 12, 13]. Stimulated by these findings, we performed an experiment to measure the angular distributions of photoelectrons from the Ar K and Kr L shells within 2–3 keV of the respective thresholds. In this brief report we present a summary of the experiment and the results. For details on the experimental procedure and the data treatment the reader may refer to the recent publications [14, 15]. Similar results for the Ne L shell have been obtained in a recent experiment [16].

PHOTOELECTRON ANGULAR DISTRIBUTIONS

The photoelectron angular distribution, described by the differential cross section $d\sigma/d\Omega$, is proportional to the square of the matrix element for photon-induced transitions between the initial state ψ_i and the final state ψ_f

$$\frac{d\sigma}{d\Omega} = f\,|\langle\psi_f \mid \exp(i\mathbf{k}\cdot\mathbf{r})\hat{\epsilon}\cdot\mathbf{p} \mid \psi_i\rangle|^2 . \qquad (1)$$

Here, $\hat{\epsilon}$ is the polarization vector of the photon, $\hbar\mathbf{k}$ the photon momentum, and $\mathbf{r}$ and $\mathbf{p}$ are the position and momentum operators of the electron. The

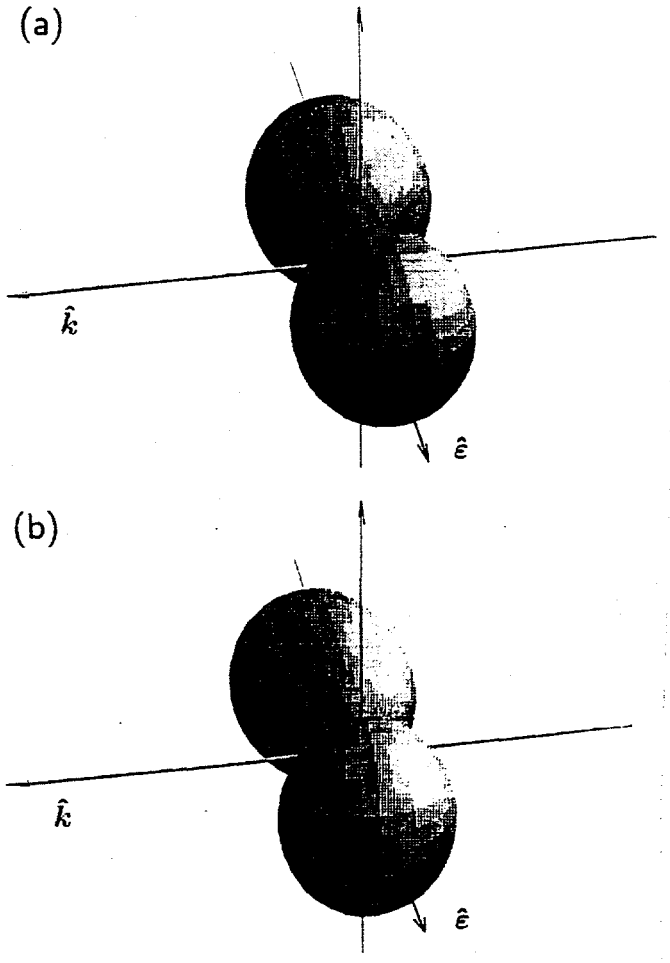

FIGURE 1. The angular distribution of photoelectrons from an s subshell. (a) dipole approximation (pure E1 interaction); (b) including the E1-E2 nondipolar contribution.

quantity f represents the combined cofactors in this expression. For simplicity, the matrix element in the following will be abbreviated by the symbol $\langle \mathcal{O} \rangle$. Employing a decomposition of the interaction with the photon in terms of electric and magnetic multipoles (cf. [17]), the transition matrix element is replaced by a sum of individual multipole transition matrix elements, $\langle \mathcal{O} \rangle = \sum_{\pi,j} \langle \pi j \rangle$. Here, the multipole transition elements are characterized by their parity π and order j. In terms of the multipole decomposition, the differential cross section breaks down into a sum of individual multipole interactions $|\langle \pi j \rangle|^2$ and cross terms of combinations $\langle \pi j \rangle \langle \pi' j' \rangle^*$ where $\pi' j' \neq \pi j$. As a result of the angular properties of the multipole components, this sum, e.g. for unpolarized

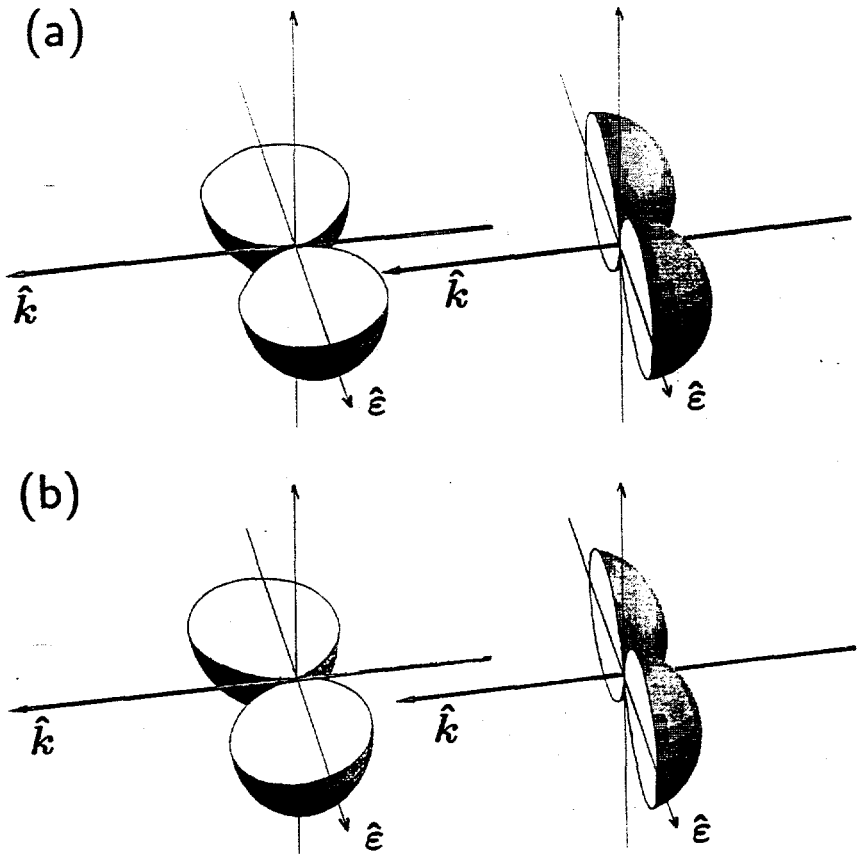

FIGURE 2. Vertical and horizontal cuts through the angular distributions depicted in FIG. 1. (a) dipole approximation (pure E1 interaction); (b) including the E1-E2 nondipolar contribution.

radiation, transforms according to[1]

$$\frac{d\sigma}{d\Omega} = f \sum_{\pi,\pi',j,j'} \langle \pi j \rangle \langle \pi' j' \rangle^* = \frac{\sigma}{4\pi} \sum_L B_L P_L(\cos\Theta). \qquad (2)$$

In this expression the angle Θ represents the emission angle of the photoelectron with respect to the photon beam. The angular integrations in a term $\langle \pi j \rangle \langle \pi' j' \rangle^*$ contribute Legendre Polynomials P_L of orders $|j - j'| \leq L \leq j + j'$, and these orders L are exclusively *even* for $\pi' = \pi$ and exclusively *odd* for $\pi' \neq \pi$. In the same manner, the corresponding radial integrations contribute to the respective coefficients B_L [11]. In Eq.(2) the B_L are normalized such that $B_0 = 1$ and $\sigma = f \sum_{\pi,j} |\langle \pi j \rangle|^2$.

[1]The corresponding expression for linearly polarized radiation contains for $L \geq 2$ additional terms $P_L^{(2)}(\cos\Theta)\cos 2\Phi$, weighted by factors B'_L. which are closely related to the parameters B_L. $P_L^{(2)}$ are second associated Legendre polynomials, and the azimuthal angle Φ is measured from the direction of linear polarization (cf. [11]).

Eq.(2) gives a convenient way of parameterizing the differential cross section with a set of angular distribution parameters B_L. The sum in L extends no further than to $2j$, with j being the highest contributing multipole order. In general the angular distribution is well described by a small number of terms, because the multipole amplitudes decrease rapidly with increasing order. The M1 and E2 interactions are smaller than the E1 interaction by a factor of $Z\alpha$, and higher multipoles are further suppressed by higher powers of $Z\alpha$. The M1 interaction acts only on the angular and spin part, but not on the spatial part of the electron's wavefunction, and thus, depending on the theoretical model, either vanishes or contributes very little. Consequently, the next-higher level of approximation to the dipole approximation includes the even-parity electric-quadrupole interaction up to terms of order $Z\alpha$ [7, 12, 13]. The parameterization of the angular distribution extends up to $L = 3$ and involves three angular distribution parameters B_1, B_2, B_3.

The angular distributions for pure E1 interaction and for E1 with additional E1-E2 interference are juxtaposed in FIG. 1 (a) and (b) for the case of ionization in an s subshell with linearly polarized x rays. It is clear that the E1 interaction is still the dominant feature in the angular distributions depicted in (b), which represents the strongest nondipolar asymmetry that has been observed in our experiment. The degree of the asymmetry can be better appreciated in the cuts through the distribution shown in FIG. 2. On the left, parts (a) and (b) each contain the cuts in the plane spanned by $\mathbf{k}$ and $\hat{\epsilon}$, and on the right the cuts in the plane perpendicular to $\mathbf{k}$ are shown. The nondipolar angular distribution is strongly asymmetric in the plane of the photon beam. In the plane perpendicular to the photon beam there is no difference between the dipolar and the nondipolar angular distributions.

EXPERIMENT

The idea pursued in the experiment was to probe the angular distribution by rotating an electron spectrometer on a circle around the polarization direction $\hat{\epsilon}$. Pure dipolar interaction results in an isotropic signal on this circle, and the nondipole effect causes an asymmetry between the forward and backward directed semicircles.

The experiment was performed using the monochromatized and highly linearly polarized x-ray beam from beamline X-24A at the National Synchrotron Light Source and an apparatus designed for angle-resolved electron spectrometry. A schematic of the experimental setup is shown in FIG. 3. The interaction region is defined by the intersection of the collimated x-ray beam and the target gas emanating from an effusive jet. A parallel-plate analyzer (PPA) is mounted such that it can be rotated on a cone with opening angle $\theta = 54.7°$.

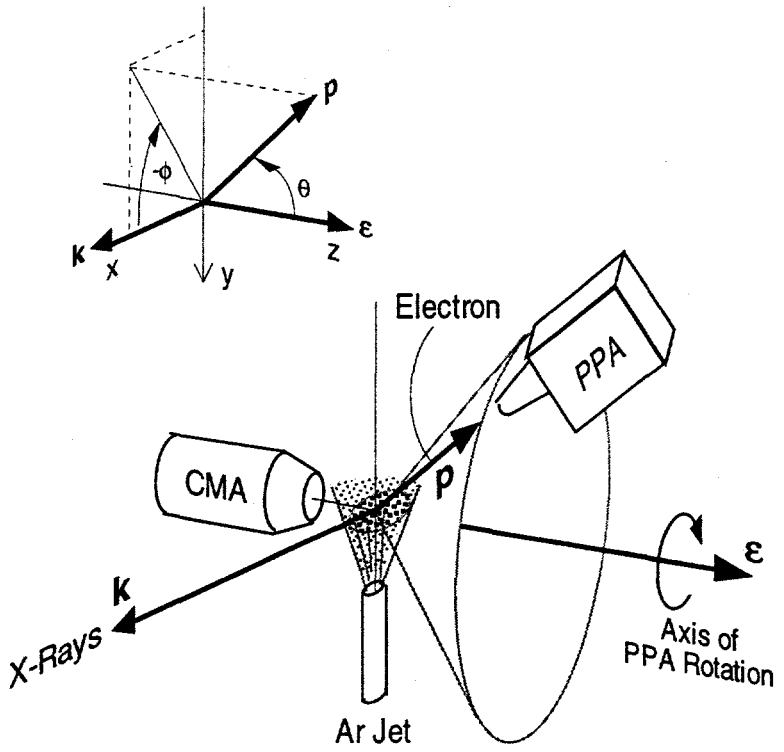

FIGURE 3. The setup of the experiment and the coordinate frame used in the representation of the angular distribution, Eq.(3). See text.

A stationary cylindrical mirror analyzer (CMA) and a downstream *p-i-n* diode (not shown in the FIG. 3) were used to monitor the target density and the photon flux during the experiment. The photoelectron intensity was recorded with the PPA-angle setting varied in 15° increments over a full 360° range. The dwell time per angle was 60–120 s, and several such angular scans were added up for each x-ray energy.

The angular distribution measured with this geometry is more conveniently represented in the system of coordinates shown in the inset of FIG. 3. In conjunction with this coordinate frame we employ an alternative parameterization to Eq.(2) and adopt the terminology for linear polarization used in Ref. [13]:

$$\frac{d\sigma}{d\Omega} = \frac{\sigma}{4\pi}\left(1 + \beta P_2(\cos\theta) + (\gamma\cos^2\theta + \delta)\sin\theta\cos\phi\right). \qquad (3)$$

The parameters β, γ, δ and the ones used in the introduction, B_1, B_2, B_3, are connected by the relations

$$\beta = -2B_2; \quad \gamma = -5B_3; \quad \delta = B_1 + B_3. \qquad (4)$$

The parameter β describes the angular anisotropy of the E1 interaction, and γ

and δ govern the nondipolar part of the angular distribution. Positive/negative values of γ and δ signify a forward/backward-directed angular distribution.

The angle θ of the experimental setup was chosen to be the so-called "magic angle", $\theta_m = 54.7°$, which is the zero of $P_2(\cos\theta)$, to remove the influence of the dipolar anisotropy parameter β on the measurement. The photoelectron intensity as a function of the azimuthal angle ϕ can then be expressed as

$$I(\theta_m, \phi) = I_0 \left(1 + \sqrt{\frac{2}{27}}(\gamma + 3\delta)\cos\phi \right). \tag{5}$$

It is clear that one can only determine a combined quantity $\gamma + 3\delta$ with this experimental geometry.

There are two instrumental effects which cause the actually observed angular distribution to deviate from the form given Eq.(5). In this brief report these will only be summarized; for a detailed description of these effects and their incorporation in the data evaluation procedure, see Ref. [15].

The first effect pertains to the inherent anisotropy of the setup depicted in FIG. 3. It is caused by the oblong source volume formed by the ~1 mm-diameter x-ray beam traversing the target gas. In order to assess this anisotropy, we measured the angular response of a variety of Auger electrons with different kinetic energies: Ar LMM, N KVV from N_2, O KVV from CO_2, Xe MNN, Ne KLL, Kr LMM, Ar KLL. Within the description of the two-step model, Auger electrons emitted in KLL transitions are emitted isotropically [18], and any nondipole terms related to the mixing of different parities, e.g. $\langle E1 \rangle \langle E2 \rangle$, vanish, rendering the remaining nondipole contributions negligible [19]. As a result, all of the measured Auger transitions should emit isotropically on the cone with opening angle equal to the magic angle. The recorded intensity variation of Auger electrons therefore represents a good measure of the instrumental anisotropy.

The second effect to cause a deviation from Eq.(5) is caused by noncomplete linear polarization of the x rays (here, $P_\perp \approx 0.95$) and by any misalignment of the experiment's rotation axis with respect to the polarization vector of the x rays (cf. [15, 20]). Even a small tilt λ between the rotation axis and the polarization vector $\hat{\epsilon}$ (here, $\lambda \approx 1°$) creates an asymmetry between the upper ($0° < \phi \leq 180°$) and lower ($180° < \phi \leq 360°$) semicircles. The dependence on λ can be essentially removed by averaging data points at azimuthal angles ϕ and $-\phi$. This procedure gives the same result as would have been obtained for a measurement with perfect alignment of the rotation axis, but with a slightly reduced degree of linear polarization, $P' = P_\perp \cos 2\lambda$. The experimental angular distribution for partially linearly polarized x rays, after correcting for the instrumental anisotropy and averaging between the upper and lower semi-

circles, has the form

$$I^{\rm av}_{P'}(\theta_m,\phi) = I_0\Big[\ 1 + \sqrt{\frac{2}{27}}(\gamma+3\delta)\cos\phi - \frac{(1-P')\beta}{4}\cos 2\phi - \frac{(1-P')\gamma}{3\sqrt{6}}\cos\phi\cos 2\phi\ \Big]. \qquad (6)$$

When using Eq.(6) as fitting function, a reasonable choice of four fitting parameters is $I_0, [\gamma+3\delta], [(1-P')\beta], [(1-P')\gamma]$, since their associated angular terms are distinctly different. In particular, the polarization-dependent terms in Eq.(6) vanish at the angles $\phi = 45°, 135°, 225°, 315°$. Just as in the case of complete linear polarization, a combined nondipole quantity $\gamma + 3\delta$ is readily obtained from such a fit without knowing the quantities P' or β. Furthermore, if the dipolar anisotropy parameter β is known, a fairly accurate determination of P' can be made. Conversely, however, the higher the degree of linear polarization and the smaller the tilt angle λ (i.e. the closer the quantity P' approaches unity), the less accurate become any evaluations of either β or γ from the fit parameters $[(1-P')\beta]$ and $[(1-P')\gamma]$, respectively.

For illustrative examples of raw data sets obtained in the angular scans, of the correction for the instrumental anisotropies, and of the corresponding fitting curves, see Refs. [14, 15].

RESULTS

The collected results of nondipolar anisotropy parameters for Ar 1*s*, Kr 2*s*, and Kr 2*p* photoionization are displayed in FIG. 4. The experimental data points are plotted as open symbols with error bars, and theoretical predictions from Refs. [12] and [13] are given for comparison as dashed and solid lines, respectively. For the level of approximation used in these calculations, i.e. including terms $\langle E1\rangle\langle E2\rangle$, the quantity δ vanishes for ionization from an *s* subshell. The results for Ar 1*s* and Kr 2*s* are therefore given in terms of the nondipole anisotropy parameter γ, whereas the results of Kr 2*p* are given as the combined quantity $\gamma + 3\delta$.

The agreement between the theoretical nonrelativistic central-field calculations and the experimental data is very good in all three cases. The experiment confirms the prediction that the nondipolar asymmetry neither approaches zero towards threshold nor is exclusively positive, as it would be expected on the basis of the simple retardation picture [6]. This difference is caused by the mutual screening of the electrons and would be absent in a simple hydrogenic model (cf. [7, 12]).

The energy dependences of γ differ considerably for the Ar 1*s* and Kr 2*s* cases (top and middle panels in FIG. 4). Ultimately, this difference is caused

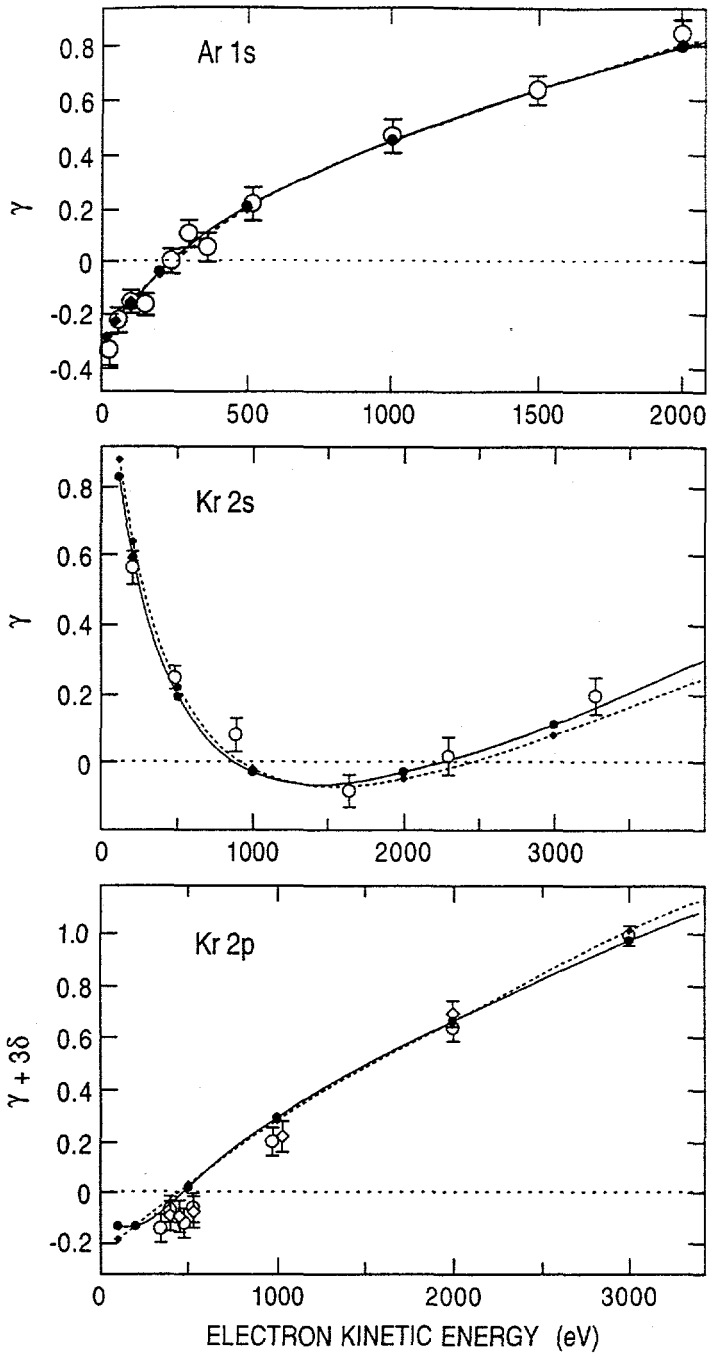

FIGURE 4. Energy dependence of the nondipole angular distribution parameter γ for Ar $1s$ (top), Kr $2s$ (middle), and of the combined quantity $\gamma + 3\delta$ for Kr $2p_j$ (bottom). Open circles/diamonds, experimental results; in the case of Kr $2p_j$ the circles and diamonds refer to the $j = 1/2$ and $j = 3/2$ fine structure components. Dashed and solid lines, theoretical predictions from [12] and [13], respectively.

by the different shapes and nodal structure of the wavefunctions in the initial states. The nondipole asymmetry parameter γ for ionization from an ns subshell can be expressed as

$$\gamma = 3k\frac{Q(ns \rightarrow \epsilon d)}{D(ns \rightarrow \epsilon p)}\cos(\delta_{\epsilon d} - \delta_{\epsilon p}). \tag{7}$$

The quantities $Q(ns \rightarrow \epsilon d)$ and $D(ns \rightarrow \epsilon p)$ are the radial quadrupole and dipole matrix elements, and $\delta_{\epsilon d}$ and $\delta_{\epsilon p}$ are the phase shifts of the continuum partial waves for quadrupole and dipole transitions, respectively. The zeros in the energy dependences for Ar $1s$ and Kr $2s$ reflect the zeros of the quadrupole matrix element and of the cosine of the phase difference. From Eq.(7) it is also clear that a zero in the dipole transition amplitude would create extremely enhanced nondipolar asymmetries.

The individual fine structure components, $j = 1/2, j = 3/2$, could be resolved in the experiment for Kr $2p$ for all but the highest energy point (bottom part of FIG. 4). No difference in the energy dependence of $\gamma + 3\delta$ for the two fine structure components was detected. The agreement between prediction and experiment is not quite as good as for Ar $1s$ and Kr $2s$. At the lower energies the experimental data points are slightly, yet systematically lower than both of the theoretical predictions. For Kr $2p$, too, backward directed nondipolar asymmetries are detected towards threshold and steadily rising positive values for increasing energies. Expressions similar to Eq.(7) for both γ and δ are given in Ref. [13]. Many more transition elements and phase differences have to be taken into account for the partial waves occurring in conjunction with the ionization from p or higher-ℓ subshells. It is an interesting observation that the two theoretical predictions agree closely in their result of $\gamma + 3\delta$, even though they obtain somewhat different results for γ and δ. For further tests of the theory, future experiments will have to make provisions that enable separate determinations of all three angular distribution parameters β, γ, δ.

OUTLOOK

As intense tunable x-ray beams ranging from 1–100 keV in energy are currently becoming available at third-generation synchrotron radiation sources in Europe, the United States, and Japan, the study of nondipole effects and their inclusion in the interpretation of photoionization data will increasingly become part of data acquisition and analysis. The nondipolar asymmetries reported in this paper, particularly in the cases of ionization from s subshells, are representative of rather straight-forward physical systems and hence the validity of nonrelativistic central-field descriptions has to some extent been expected. Just as for determinations of the β parameter in the electric-dipole interaction, it is

the less straight-forward situations, for example the nondipolar asymmetries in the threshold region, in the regions of resonances [7] and of Cooper minima [21], which represent interesting subjects for future experimental and theoretical investigations. The information derived from the electric-quadrupole interaction is complementary to that obtained from electric-dipole interaction, because the atomic wavefunction is probed in a different way. In addition, relativistic effects gain importance in studies with higher-Z elements and higher x-ray energies. Even at relatively low photon energies the effect of the electric-quadrupole interaction should be observable when, e.g., in a resonance, the electric-dipole amplitude is strongly suppressed or the electric-quadrupole amplitude strongly enhanced. Such experiments, be it at high photon energies where the photoionization cross section decreases or in cases where the dominant electric-dipole contribution is suppressed, will be faced with the problem of very low counting rates. Progress in this field will therefore strongly profit from instrumental developments which increase the efficiency in angular distribution measurements.

ACKNOWLEDGMENTS

We thank C. A. Kurtz and B. J. Zabransky for excellent technical support. We are indebted to P. M. Dehmer, J. L. Dehmer, and R. D. Deslattes for the loan of equipment. We are especially thankful to M. Peshkin for helpful suggestions and illuminating discussions. Measurements were carried out at the National Synchrotron Light Source, Brookhaven National Laboratory, which is supported by the U.S. Department of Energy, Division of Materials Sciences and Chemical Sciences. This work was supported by the U.S. Department of Energy Office of Basic Sciences under Contract W-31-109-Eng-38.

REFERENCES

[1] A. F. Starace, in *Handbuch der Physik*, edited by W. Mehlhorn (Springer-Verlag, Berlin, 1982), Vol. XXXI, pp. 1–121.

[2] V. Schmidt, Rep. Prog. Phys. **55**, 1483 (1992).

[3] W. Bothe, Z. Phys. **26**, 59 (1924).

[4] P. Auger and F. Perrin, Journal de Physique **6**, 93 (1927).

[5] A. Sommerfeld and G. Schur, Ann. d. Phys. **4**, 309 (1930).

[6] H. A. Bethe and E. E. Salpeter, *Quantum Mechanics of One- and Two-Electron Atoms* (Springer-Verlag, Berlin, 1957).

[7] M. Ya. Amusia, P. U. Arifov, A. S. Baltenkov, A. A. Grinberg, and S. G. Shapiro, Phys. Lett. **47A**, 66 (1974); M. Y. Amusia and N. A. Cherepkov, in *Case Studies in Atomic Physics* (North-Holland, Amsterdam, 1975), Vol. 5, pp. 47–179; M. Ya. Amus'ya, V. K. Dolmatov, and V. K. Ivanov, Sov. Phys. Tech. Phys. **31**(1), 4 (1986), and references therein.

[8] R. H. Pratt, A. Ron, H. K. Tseng, Rev. Mod. Phys. **45**, 273 (1973); A. Ron, R. H. Pratt, and H. K. Tseng, Chem. Phys. Lett. **47**, 377 (1977); Y. S. Kim, R. H. Pratt, A. Ron, H. K. Tseng, Phys. Rev. A **22**, 567 (1980).

[9] M. O. Krause, Phys. Rev. **177**, 151 (1969); F. Wuilleumier and M. O. Krause, Phys. Rev. A **10**, 242 (1974).

[10] H. K. Tseng, R. H. Pratt, S. Yu, and A. Ron, Phys. Rev. A **17**, 1061 (1978).

[11] J. H. Scofield, Phys. Rev. A **40**, 3054 (1989); Phys. Scr. **41**, 59 (1990).

[12] A. Bechler and R. H. Pratt, Phys. Rev. A **39**, 1774 (1989); Phys. Rev. A **42**, 6400 (1990).

[13] J. W. Cooper, Phys. Rev. A **42**, 6942 (1990); Phys. Rev. A **45**, 3362 (1990); Phys. Rev. A **47**, 1841 (1993).

[14] B. Krässig *et al.*, Phys. Rev. Lett. **75**, 4736 (1995).

[15] M. Jung *et al.*, Phys. Rev. A **54**, 2127 (1996).

[16] O. Hemmers *et al.*, 1996, to be published.

[17] M. Peshkin, Adv. Chem. Phys. **18**, 1 (1970).

[18] B. Cleff and W. Mehlhorn, J. Phys. B: Atom. Molec. Phys. **7**, 593 (1974); E. G. Berezhko and N. M. Kabachnik, J. Phys. B: Atom. Molec. Phys. **10**, 2467 (1977).

[19] N. M. Kabachnik and I. P. Sazhina, 1996, to be published.

[20] P.-S. Shaw, U. Arp, and S. Southworth, Phys. Rev. A **54**, 1463 (1996).

[21] M. S. Wang, Y. S. Kim, R. H. Pratt, and A. Ron, Phys. Rev. A **25**, 857 (1982).